

Gaussian and plane-wave mixed density fitting for periodic systems

Qiming Sun,^{*,†} Timothy C. Berkelbach,[‡] James D. McClain,[¶] and Garnet Kin-Lic Chan^{*,†}

[†]*Division of Chemistry and Chemical Engineering, California Institute of Technology, CA 91125*

[‡]*Department of Chemistry and James Franck Institute, University of Chicago, Chicago, IL 60637*

[¶]*Department of Chemistry, Princeton University, Princeton, NJ 08543*

E-mail: osirpt.sun@gmail.com; gkc1000@gmail.com

Abstract

We introduce a mixed density fitting scheme that uses both a Gaussian and a plane-wave fitting basis to accurately evaluate electron repulsion integrals in crystalline systems. We use this scheme to enable efficient all-electron Gaussian based periodic density functional and Hartree-Fock calculations.

1 Introduction

Computing the two-electron repulsion integrals (ERIs)

$$(\mu\nu|\kappa\lambda) = \int \mu^*(\mathbf{r}_1)\nu(\mathbf{r}_1)\frac{1}{r_{12}}\kappa^*(\mathbf{r}_2)\lambda(\mathbf{r}_2)d\mathbf{r}_1d\mathbf{r}_2 \quad (1)$$

has been a traditional bottleneck in electronic structure modeling when using a Gaussian basis. The ERIs serve both as final targets of computation, or may be used in contractions to form intermediates, such as in the Coulomb and exchange operators in mean-field calculations.

Various approximations have been proposed to reduce the cost of ERI computation and their associated intermediates in both molecular and crystalline systems. Many of them, including Gaussian density fitting,¹⁻⁵ Cholesky decomposition,⁶⁻⁸ plane-wave Fourier transform techniques,⁹⁻¹³ and the pseudo-spectral method and its variants,^{14,15} can be considered to fall under the general rubric of density fitting (DF) methods. Density fitting can be used both when computing individual ERIs, as well as in intermediate formation. The basic idea is to approximate the two-center atomic orbital pair density in Eq. (1) with an expansion in auxiliary functions, the fitting basis. The approximate density ρ' is obtained by minimizing its distance to the reference two-center density ρ with respect to a metric $g(\mathbf{r}_1, \mathbf{r}_2)$ (such as the Coulomb metric r_{12}^{-1} or overlap metric $\delta(\mathbf{r}_1 - \mathbf{r}_2)$)

$$\min_{\rho'} \iint [\rho(\mathbf{r}_1) - \rho'(\mathbf{r}_1)] g(\mathbf{r}_1, \mathbf{r}_2) [\rho(\mathbf{r}_2) - \rho'(\mathbf{r}_2)] d\mathbf{r}_1 d\mathbf{r}_2$$

By choosing different metrics and fitting bases, one recovers the different schemes mentioned above. However, the most common version of DF uses a Gaussian fitting basis, in conjunction with the Coulomb metric. We will refer to this standard combination of fitting basis and Coulomb metric as Gaussian density fitting (GDF). Gaussian density fitting is available in almost all the major quantum chemistry packages today.^{3-5,16-24}

In this work, we extend the Gaussian DF methodology to a *mixed basis* density fitting (MDF). This creates an efficient DF framework well suited to the all-electron modeling of periodic systems. The basic idea in MDF is to use a mixed auxiliary basis of Gaussians

$\chi_Q(\mathbf{r})$ and plane-waves (PW), expanding the density as

$$\rho(\mathbf{r}) = \sum_Q \chi_Q(\mathbf{r}) d_Q + \sum_{\mathbf{G}} e^{i\mathbf{G}\cdot\mathbf{r}} c_{\mathbf{G}} \quad (2)$$

The mixed-basis representation allows the representation of compact densities through the Gaussian functions $\chi_Q(\mathbf{r})$, while offering systematic convergence for smooth densities through the PWs. These two properties address the challenges of Coulomb evaluation in all-electron periodic calculations, where contributions from both the core and diffuse interstitial densities must be efficiently computed. Further, the use of a PW representation provides a natural way to handle the Coulomb divergence that appears in periodic settings. Although such all-electron calculations can be expected to be more expensive than pseudo-potential calculations, they allow us to carry out computations free of pseudo-potential error.

There are related works in the literature. These include the Gaussian and (augmented) plane-wave formalism by Parrinello and coworkers,^{11,25,26} and the Fourier transform Coulomb method of Füsti-Molnár and Pulay.^{9,27} In both of these, Gaussian basis sets are used to expand the orbitals, and the density matrix contributions of Gaussians with large exponents (compact Gaussians) and small exponents (smooth Gaussians) are separated. The Coulomb potential and energy contributions of the smooth Gaussians are evaluated by PW density fitting using the FFT, while the compact Gaussian ERIs are evaluated explicitly. Thus, unlike in our mixed density fitting, Gaussian density fitting is not used at all. Further, both works are concerned with optimizing the evaluation of the Coulomb potential and energy only, rather than the more general ERI kernel, as used in the computation of exchange and in many-body methods. Some other differences include the manner in which compact and smooth densities are partitioned, as well as our use of analytical Fourier transforms to achieve higher accuracy than the FFT with the same number of PW's. The impact of these choices will become apparent in the benchmark applications discussed below.

The rest of this manuscript describes in detail the implementation of the mixed density

fitting scheme and its benchmarking. In sections 2.1 and 2.2 we present the formulae to compute the 4-index ERIs in terms of the MDF mixed Gaussian and PW fitting basis. The procedure to carry out GDF in a periodic system, which serves as a comparison for MDF, is discussed in section 2.3 using some formulae developed in the MDF framework. The MDF scheme is benchmarked for the all-electron Coulomb, exchange, and total energy at the Hartree-Fock level, and the all-electron band structure at the density functional level, for some simple crystals in section 3. Our conclusions are presented in section 4.

2 Theory

2.1 Mixed density fitting method for periodic systems

In an N -cell crystalline system, the AO functions $\phi_\mu(\mathbf{r})$ are translational-symmetry-adapted linear combinations of Gaussian atomic orbitals $\mu(\mathbf{r})$ ²⁸

$$\phi_\mu(\mathbf{r}) = \sum_{\mathbf{T}} e^{i\mathbf{k}_\mu \cdot \mathbf{T}} \mu(\mathbf{r} - \mathbf{T}) \quad (3)$$

where \mathbf{T} is a translation vector and \mathbf{k}_μ is a crystal momentum vector. In the mixed density fitting scheme, the AO products $\rho_{\mu\nu}(\mathbf{r})$ are approximated by an expansion of periodic Gaussian fitting functions plus plane-wave functions

$$\rho_{\mu\nu}(\mathbf{r}) = \phi_\mu^*(\mathbf{r})\phi_\nu(\mathbf{r}) = \sum_Q \phi_Q^{\mathbf{k}_{\mu\nu}}(\mathbf{r})d_{Q,\mu\nu} + \sum_{\mathbf{G}+\mathbf{k}_{\mu\nu} \neq 0} \frac{e^{i(\mathbf{G}+\mathbf{k}_{\mu\nu}) \cdot \mathbf{r}}}{\sqrt{N\Omega}} c_{\mathbf{G},\mu\nu} + \bar{\rho}_{\mu\nu}, \quad (4)$$

where $\mathbf{k}_{\mu\nu} = -\mathbf{k}_\mu + \mathbf{k}_\nu$. $N\Omega$ represents the total volume of the computational crystal and Ω is the volume of the unit cell. The fitting function $\phi_Q^{\mathbf{k}}(\mathbf{r})$ is defined as

$$\phi_Q^{\mathbf{k}}(\mathbf{r}) = \chi_Q^{\mathbf{k}}(\mathbf{r}) - \xi_Q^{\mathbf{k}}(\mathbf{r}) = \frac{1}{\sqrt{N}} \sum_{\mathbf{T}} e^{i\mathbf{k} \cdot \mathbf{T}} [\chi_Q(\mathbf{r} - \mathbf{T}) - \xi_Q(\mathbf{r} - \mathbf{T})], \quad (5)$$

$$\chi_Q^{\mathbf{k}}(\mathbf{r}) = \frac{1}{\sqrt{N}} \sum_{\mathbf{T}} e^{i\mathbf{k} \cdot \mathbf{T}} \chi_Q(\mathbf{r} - \mathbf{T}), \quad (6)$$

$$\xi_Q^{\mathbf{k}}(\mathbf{r}) = \frac{1}{\sqrt{N}} \sum_{\mathbf{T}} e^{i\mathbf{k} \cdot \mathbf{T}} \xi_Q(\mathbf{r} - \mathbf{T}), \quad (7)$$

Here, $\chi_Q(\mathbf{r})$ is a compact Gaussian fitting function, and $\xi_Q(\mathbf{r})$ is a smooth Gaussian fitting function which is subtracted from it to ensure that the fitting basis functions carry zero net charge and zero multipoles. For example, for a p -type auxiliary function, we require that the dipole integral vanishes

$$\int \mathbf{r} [\chi_p(\mathbf{r}) - \xi_p(\mathbf{r})] d\mathbf{r} = 0. \quad (8)$$

The Coulomb potential of a zero-charge and zero-multipole density decays exponentially in real space, and this allows us to compute the Coulomb integrals of the Gaussian fitting functions using lattice summation. The compensating function $\xi_Q(\mathbf{r})$ does not hold any other physical significance, but should be chosen to be smooth so that its contributions can be efficiently compensated for in the PW expansion. Given a real space lattice sum truncation distance, the smoothness of $\xi_Q(\mathbf{r})$ can be optimized in the same manner as is done in the optimization of the Ewald parameter.^{29,30} Because the charge is excluded from the Gaussian fitting basis, we handle it as part of the PW expansion, and this is the last term in Eq. (4) (corresponding to $\mathbf{G} = 0$ and $\mathbf{k}_\mu = \mathbf{k}_\nu$)

$$\bar{\rho}_{\mu\nu} = \frac{1}{N\Omega} \int \phi_\mu^*(\mathbf{r}) \phi_\nu(\mathbf{r}) d\mathbf{r} = \frac{S_{\mu\nu}}{\Omega} \quad (9)$$

where

$$S_{\mu\nu} = \sum_{\mathbf{T}} e^{i\mathbf{k}_\nu \cdot \mathbf{T}} \int \mu^*(\mathbf{r}) \nu(\mathbf{r} - \mathbf{T}) d\mathbf{r} \quad (10)$$

is the AO overlap integral (per unit cell).

The fitting coefficients are obtained by minimizing the density fitting error in the Coulomb

metric. This leads to a linear equation for the coefficients $d_{Q,\mu\nu}$ and $c_{\mathbf{G},\mu\nu}$

$$\begin{pmatrix} (\phi_P^{-\mathbf{k}_{\mu\nu}} | \phi_Q^{\mathbf{k}_{\mu\nu}}) & \frac{4\pi\rho_P(-\mathbf{G}-\mathbf{k}_{\mu\nu})}{\sqrt{\Omega}|\mathbf{G}+\mathbf{k}_{\mu\nu}|^2} \\ \frac{4\pi\rho_Q(\mathbf{G}+\mathbf{k}_{\mu\nu})}{\sqrt{\Omega}|\mathbf{G}+\mathbf{k}_{\mu\nu}|^2} & \frac{4\pi}{|\mathbf{G}+\mathbf{k}_{\mu\nu}|^2} \end{pmatrix} \begin{pmatrix} d_{Q,\mu\nu} \\ c_{\mathbf{G},\mu\nu} \end{pmatrix} = \begin{pmatrix} \sqrt{N} [(\phi_P^{-\mathbf{k}_{\mu\nu}} | \phi_\mu \phi_\nu) - \bar{V}_P^{-\mathbf{k}_{\mu\nu}} \bar{\rho}_{\mu\nu}] \\ \frac{4\pi\rho_{\mu\nu}(\mathbf{G}+\mathbf{k}_{\mu\nu})}{\sqrt{\Omega}|\mathbf{G}+\mathbf{k}_{\mu\nu}|^2} \end{pmatrix} \quad (11)$$

where the integrals (derived in Appendix A) are

$$(\phi_P^{-\mathbf{k}} | \phi_Q^{\mathbf{k}}) = \sum_{\mathbf{T}} e^{i\mathbf{k}\cdot\mathbf{T}} \int [\chi_P(\mathbf{r}_1) - \xi_P(\mathbf{r}_1)] \frac{1}{r_{12}} [\chi_Q(\mathbf{r}_2 - \mathbf{T}) - \xi_Q(\mathbf{r}_2 - \mathbf{T})] d\mathbf{r}_1 d\mathbf{r}_2 \quad (12)$$

$$\rho_Q(\mathbf{G} + \mathbf{k}) = \int e^{-i(\mathbf{G}+\mathbf{k})\cdot\mathbf{r}} [\chi_Q(\mathbf{r}) - \xi_Q(\mathbf{r})] d\mathbf{r} \quad (13)$$

$$\bar{V}_P^{\mathbf{k}} = \begin{cases} \frac{\pi}{\alpha_{P_\xi}} - \frac{\pi}{\alpha_{P_\chi}} & \mathbf{k} = 0 \text{ and } \chi_P \in \text{s-type GTOs} \\ 0 & \text{otherwise} \end{cases} \quad (14)$$

$$(\phi_P^{-\mathbf{k}_{\mu\nu}} | \phi_\mu \phi_\nu) = \sum_{\mathbf{T}_\mu \mathbf{T}_\nu} e^{i\mathbf{k}_\nu \cdot \mathbf{T}_\nu - i\mathbf{k}_\mu \cdot \mathbf{T}_\mu} \int [\chi_P(\mathbf{r}_1) - \xi_P(\mathbf{r}_1)] \frac{1}{r_{12}} \mu^*(\mathbf{r}_2 - \mathbf{T}_\mu) \nu(\mathbf{r}_2 - \mathbf{T}_\nu) d\mathbf{r}_1 d\mathbf{r}_2 \quad (15)$$

$$\rho_{\mu\nu}(\mathbf{G} + \mathbf{k}_{\mu\nu}) = \sum_{\mathbf{T}} e^{i\mathbf{k}_\nu \cdot \mathbf{T}} \int e^{-i(\mathbf{G}+\mathbf{k}_{\mu\nu})\cdot\mathbf{r}} \mu^*(\mathbf{r}) \nu(\mathbf{r} - \mathbf{T}) d\mathbf{r} \quad (16)$$

In Eq. (14), α_{P_χ} and α_{P_ξ} are the exponents of the Gaussian functions $\chi_P(\mathbf{r})$ and $\xi_P(\mathbf{r})$. In the above integrals, computing the three center integral (15) is demanding due to the double lattice sum, with a cost of $O(n^2 m N_c^2)$ where n is the number of AOs, m is the number of auxiliary Gaussian functions and N_c is the number of images in the lattice summation.

Eqs. (13) and (16) involve the Fourier transforms of the fitting Gaussians and AO products. While one can approximate these integrals using a discrete fast Fourier transform (FFT), this is only practical if the Gaussians involved are not very steep, as for example, in pseudo-potential calculations; otherwise prohibitively large Fourier grids are necessary (see section 3). Alternatively, the integrals can be calculated analytically. The formulae for the analytical Fourier transforms are documented in Appendix B. The leading computational cost is for the AO products which has a formal scaling of $O(n^2 N_G N_c)$ where N_G is the num-

ber of PWs. Although there is only one factor of N_c (compared to the three center Gaussian integrals) the analytical Fourier transforms also become expensive for a large number of PWs. However, as long as the Gaussian fitting functions of core and valence characters are appropriately tuned, it is not difficult to require only a modest number of PWs in the MDF expansion of the smooth part of the density. The analytical Fourier transform technique can be used in both pseudo-potential and all-electron calculations. As the PWs in this approach are strictly used only to represent the density and not to numerically sample the Gaussians, one can use fewer PWs with the analytical Fourier transform than in a typical FFT-driven calculation.

Finally, when defining ERIs in a periodic system, we remove the net charge of the AO product to avoid the divergent Coulomb contribution, corresponding to removing the $\mathbf{G} = 0$ singularity when $\mathbf{k}_{\mu\nu} = 0$.³¹ (The $\mathbf{G} = 0$ electronic contribution, which only depends on the number of electrons in the unit cell, is appropriately handled together with the electron-nuclear and nuclear-nuclear $\mathbf{G} = 0$ contributions, yielding an additive constant to the total energy.³¹) Using the quantities defined in the MDF expansion, the periodic ERI (here, and in the following text, per unit cell) is assembled as

$$\begin{aligned}
(\mu\nu|\kappa\lambda) &= \frac{1}{N} \int \frac{[\phi_\mu(\mathbf{r}_1)\phi_\nu(\mathbf{r}_1) - \bar{\rho}_{\mu\nu}][\phi_\kappa(\mathbf{r}_2)\phi_\lambda(\mathbf{r}_2) - \bar{\rho}_{\kappa\lambda}]}{r_{12}} d\mathbf{r}_1 d\mathbf{r}_2 \\
&= \sum_Q \frac{d_{Q,\mu\nu}}{\sqrt{N}} (\phi_Q^{\mathbf{k}_{\mu\nu}} | \phi_\kappa \phi_\lambda) - \bar{\rho}_{\kappa\lambda} \sum_Q \frac{d_{Q,\mu\nu}}{\sqrt{N}} \bar{V}_Q^{\mathbf{k}_{\mu\nu}} + \sum_{\mathbf{G}+\mathbf{k}_{\mu\nu} \neq 0} c_{\mathbf{G},\mu\nu} \rho_{\kappa\lambda}(-\mathbf{G} + \mathbf{k}_{\kappa\lambda}) \quad (17)
\end{aligned}$$

In the ERI expression, crystal momentum conservation is used

$$(-\mathbf{k}_\mu + \mathbf{k}_\nu - \mathbf{k}_\kappa + \mathbf{k}_\lambda) \cdot \mathbf{a} = 2n\pi \quad (18)$$

where \mathbf{a} is the lattice vector.

2.2 Linear dependence in the MDF fitting basis

In the mixed fitting basis, the periodic Gaussian functions and PWs may become linearly dependent with respect to each other as each subset becomes increasingly complete. In practice, this causes numerical instabilities when solving the linear equation in the form (11) directly. To remove the linear dependencies, we orthogonalize the fitting functions with respect to the Coulomb metric through the transformation

$$\begin{pmatrix} \phi_Q^{\mathbf{k}}(\mathbf{r}) & \frac{e^{i(\mathbf{G}+\mathbf{k})\cdot\mathbf{r}}}{\sqrt{N\Omega}} \end{pmatrix} \begin{pmatrix} \mathbf{t}^{\mathbf{k}} & 0 \\ -\frac{\rho_Q(\mathbf{G}+\mathbf{k})}{\sqrt{\Omega}}\mathbf{t}^{\mathbf{k}} & \frac{|\mathbf{G}+\mathbf{k}|}{2\sqrt{\pi}} \end{pmatrix} \quad (19)$$

where the rectangular matrix $\mathbf{t}^{\mathbf{k}}$ is the transformation to diagonalize the dressed Coulomb matrix of the Gaussian fitting functions

$$\tilde{J}_{PQ}^{\mathbf{k}} = (\phi_P^{-\mathbf{k}}|\phi_Q^{\mathbf{k}}) - \sum_{\mathbf{G}+\mathbf{k}\neq 0} \frac{4\pi\rho_P(-\mathbf{G}-\mathbf{k})\rho_Q(\mathbf{G}+\mathbf{k})}{\Omega|\mathbf{G}+\mathbf{k}|^2} \quad (20)$$

$$\mathbf{t}^{\mathbf{k}\dagger}\tilde{\mathbf{J}}^{\mathbf{k}}\mathbf{t}^{\mathbf{k}} = \mathbf{1} \quad (21)$$

Although different choices can be made to remove linear dependencies, different schemes do not share the same numerical stability. We used the transformation (19) because it does not mix Gaussian functions into the PWs. An advantage of the PW basis is that the Coulomb operator is diagonal in the PW representation. Manipulating the basis orthogonalization in this diagonal representation is straightforward and numerically stable, leading to the normalization factor $|\mathbf{G}+\mathbf{k}|/2\sqrt{\pi}$ in Eq. (19). Projecting the PWs out of the Gaussian functions in (20) leads to a highly singular matrix. To remove the linear dependence of the Gaussian functions, we diagonalize this singular matrix and remove the eigenvectors associated with small eigenvalues below a threshold. The effect of the linear dependence threshold on the stability of the results is tested in Section 3. In our program, we use a default threshold of 10^{-7} .

Applying transformation (19) to the linear equation (11) followed by removal of small eigenvalues allows us to stably determine the density fitting coefficients. With respect to the transformed fitting functions, we can define a new MDF expression for the ERIs in (17)

$$(\mu\nu|\kappa\lambda) = \sum_i L_{i,\mu\nu} L_{i,\kappa\lambda} + \sum_{\mathbf{G}+\mathbf{k}_{\mu\nu} \neq 0} \frac{4\pi \rho_{\mu\nu}(\mathbf{G} + \mathbf{k}_{\mu\nu}) \rho_{\kappa\lambda}(-\mathbf{G} + \mathbf{k}_{\kappa\lambda})}{\Omega |\mathbf{G} + \mathbf{k}_{\mu\nu}|^2} \quad (22)$$

$$L_{i,\mu\nu} = \sum_P t_{Pi}^{\mathbf{k}_{\mu\nu}*} \left[(\phi_P^{-\mathbf{k}_{\mu\nu}} | \phi_\mu \phi_\nu) - \bar{V}_P^{-\mathbf{k}_{\mu\nu}} \bar{\rho}_{\mu\nu} - \sum_{\mathbf{G}+\mathbf{k}_{\mu\nu} \neq 0} \frac{4\pi \rho_P(-\mathbf{G} - \mathbf{k}_{\mu\nu}) \rho_{\mu\nu}(\mathbf{G} + \mathbf{k}_{\mu\nu})}{\Omega |\mathbf{G} + \mathbf{k}_{\mu\nu}|^2} \right] \quad (23)$$

2.3 Gaussian density fitting for periodic systems

In the current work, we will benchmark mixed density fitting against standard Gaussian density fitting. We first describe how GDF may be efficiently implemented in periodic systems using some of the results introduced above for MDF. In the periodic setting, the AO products in the standard GDF method are expanded in a set of periodic Gaussian fitting functions

$$\rho_{\mu\nu} = \sum_Q \chi_Q^{\mathbf{k}_{\mu\nu}}(\mathbf{r}) d_{Q,\mu\nu}. \quad (24)$$

The Coulomb metric when used directly in the periodic setting diverges. Thus, we exclude the net charge of the AO products in the fitting expansion

$$\rho_{\mu\nu}(\mathbf{r}) - \bar{\rho}_{\mu\nu} = \sum_Q \left(\chi_Q^{\mathbf{k}_{\mu\nu}}(\mathbf{r}) - \bar{\chi}_Q^{\mathbf{k}_{\mu\nu}} \right) d_{Q,\mu\nu}. \quad (25)$$

$$\bar{\chi}_Q^{\mathbf{k}} = \begin{cases} \frac{\sqrt{N}}{\Omega} & \mathbf{k} = 0 \text{ and } \chi_Q(\mathbf{r}) \in s\text{-type GTOs} \\ 0 & \text{otherwise} \end{cases} \quad (26)$$

The two-electron integrals can then be formulated in terms of the GDF quantities as

$$(\mu\nu|\kappa\lambda) = \sum_i \mathcal{V}_{P,\mu\nu}(\mathcal{J}^{-1})_{PQ} \mathcal{V}_{Q,\kappa\lambda} \quad (27)$$

$$\mathcal{V}_{P,\mu\nu} = \frac{1}{\sqrt{N}} (\chi_P^{\mathbf{k}_{\nu\mu}} - \bar{\chi}_P^{\mathbf{k}_{\nu\mu}} | \phi_\mu \phi_\nu - \bar{\rho}_{\mu\nu}) \quad (28)$$

$$\mathcal{J}_{PQ} = (\chi_P^{\mathbf{k}_{\nu\mu}} - \bar{\chi}_P^{\mathbf{k}_{\nu\mu}} | \chi_Q^{\mathbf{k}_{\mu\nu}} - \bar{\chi}_Q^{\mathbf{k}_{\mu\nu}}) \quad (29)$$

The two-center and three-center Coulomb integrals represent Coulomb interactions between chargeless density distributions and thus are not divergent in the real space lattice summation, however the convergence may be very slow or even conditional on the summation order. To accelerate the lattice summation, we can insert a compensating function $\xi^{\mathbf{k}}(\mathbf{r})$ in the density fitting expansion that removes higher multipoles of $\chi_Q^{\mathbf{k}}(\mathbf{r})$ as in the MDF procedure,

$$\begin{aligned} \rho_{\mu\nu}(\mathbf{r}) - \bar{\rho}_{\mu\nu} &= \sum_Q \left(\chi_Q^{\mathbf{k}_{\mu\nu}}(\mathbf{r}) - \xi_Q^{\mathbf{k}_{\mu\nu}}(\mathbf{r}) + \xi_Q^{\mathbf{k}_{\mu\nu}}(\mathbf{r}) - \bar{\chi}_Q^{\mathbf{k}_{\mu\nu}} \right) d_{Q,\mu\nu} \\ &= \sum_Q \phi_Q^{\mathbf{k}_{\mu\nu}}(\mathbf{r}) d_{Q,\mu\nu} + \sum_Q \left(\xi_Q^{\mathbf{k}_{\mu\nu}}(\mathbf{r}) - \bar{\chi}_Q^{\mathbf{k}_{\mu\nu}} \right) d_{Q,\mu\nu}, \end{aligned} \quad (30)$$

This allows us to efficiently compute the two-center and three-center integrals in a two-step scheme: first we evaluate the integrals involving $\phi_Q(\mathbf{r})$ using real space lattice summation; then the remaining contributions are evaluated using a PW expansion. With this scheme, the integrals (28) and (29) are obtained as

$$\mathcal{V}_{P,\mu\nu} = (\phi_P^{-\mathbf{k}_{\mu\nu}} | \phi_\mu \phi_\nu) - \bar{V}_P^{-\mathbf{k}_{\mu\nu}} \bar{\rho}_{\mu\nu} + \sum_{\mathbf{G}+\mathbf{k}_{\mu\nu} \neq 0} \frac{4\pi \rho_{\xi_P}(-\mathbf{G} - \mathbf{k}_{\mu\nu}) \rho_{\mu\nu}(\mathbf{G} + \mathbf{k}_{\mu\nu})}{\Omega |\mathbf{G} + \mathbf{k}_{\mu\nu}|^2} \quad (31)$$

$$\begin{aligned} \mathcal{J}_{PQ} &= (\phi_P^{-\mathbf{k}_{\mu\nu}} | \phi_Q^{\mathbf{k}_{\mu\nu}}) + \sum_{\mathbf{G}+\mathbf{k}_{\mu\nu} \neq 0} \frac{4\pi \rho_{\xi_P}(-\mathbf{G} - \mathbf{k}_{\mu\nu}) \rho_Q(\mathbf{G} + \mathbf{k}_{\mu\nu})}{\Omega |\mathbf{G} + \mathbf{k}_{\mu\nu}|^2} \\ &+ \sum_{\mathbf{G}+\mathbf{k}_{\mu\nu} \neq 0} \frac{4\pi \rho_P(-\mathbf{G} - \mathbf{k}_{\mu\nu}) \rho_{\xi_Q}(\mathbf{G} + \mathbf{k}_{\mu\nu})}{\Omega |\mathbf{G} + \mathbf{k}_{\mu\nu}|^2} + \sum_{\mathbf{G}+\mathbf{k}_{\mu\nu} \neq 0} \frac{4\pi \rho_{\xi_P}(-\mathbf{G} - \mathbf{k}_{\mu\nu}) \rho_{\xi_Q}(\mathbf{G} + \mathbf{k}_{\mu\nu})}{\Omega |\mathbf{G} + \mathbf{k}_{\mu\nu}|^2} \end{aligned} \quad (32)$$

where

$$\rho_{\xi_P}(\mathbf{G} + \mathbf{k}) = \int e^{-i(\mathbf{G}+\mathbf{k})\cdot\mathbf{r}} \xi_P(\mathbf{r}) d\mathbf{r} \quad (33)$$

Note that in the GDF calculations, *we always use sufficient number of PWs to completely converge the PW representation of the compensating Gaussian*. This ensures that the GDF calculations are a measure purely of the quality of the original Gaussian density fitting basis.

3 Benchmarking MDF

We have implemented the MDF method as described above in our electronic structure program package PySCF.³² To test the accuracy of the MDF method, we first computed the Γ -point Hartree-Fock Coulomb (E_J) and exchange energies (E_K) for the hydrogen crystal (cubic unit cell in $Fd\bar{3}m$ symmetry, lattice parameter $a = 3.567$ Å, cc-pVDZ basis). The MDF Gaussian fitting basis was the even tempered basis (ETB) 10s6p2d (see Table 1). The compensating Gaussians (see Eq. (5)) were chosen to have exponent 0.2. The PW basis was constructed from a uniform reciprocal grid. The real-space lattice summation was truncated at a distance of 9.2 Å. This ensured that both the AO basis and auxiliary Gaussian basis lattice sums were fully converged.

We compare the different kinds of density fitting in Figures 1a and 1b. Using pure GDF and the large even tempered fitting basis, we can fit E_J to roughly 0.1 m E_h accuracy and E_K to roughly 1 m E_h accuracy. Note that the H atom cc-pVDZ basis does not contain any steep Gaussian functions. This means it is also practical in this system to use only PWs as the fitting functions. We show the results of PW density fitting (labelled FFT) where the PW coefficients and contributions are determined by FFT. The PW density fitting converges the Coulomb and exchange energy very systematically as a function of the number of PWs. This demonstrates the strength of including PWs in the fitting basis, and in fact we use the systematic convergence to estimate the reference Coulomb and exchange energies. Finally, we observe the effect of using both Gaussians and PWs in the MDF expansion (labelled MDF-

AFT). We see that introducing the Gaussian fitting basis leads to improved convergence relative to the pure PW expansion. The MDF expansion is 4-5 orders of magnitude more accurate than the pure PW expansion with the same number of PWs. The accuracy of GDF itself is close to the accuracy of MDF with a minimal PW basis (27 PWs, 1 grid point per direction). Since the difference between the Gaussian fitting basis in GDF and MDF is the set of compensating Gaussian functions in MDF, this reflects the fact that the compensating Gaussians used in MDF are here well represented by a small number of PWs. Further, adding a modest number of PWs in MDF significantly improves the accuracy over pure GDF, for example, 729 PWs (9 per axis) reduces the fitting error to $0.1 \mu E_h$.

In the MDF-AFT results, we used analytical Fourier transforms for all PW-related integrals in the MDF method. As discussed in the methods section, it is also possible to use the discrete FFT to compute these integrals, although additional errors are expected. Note that there are three equations (20), (22) and (23) that involve quantities in reciprocal space. FFT cannot be used to obtain the reciprocal space densities in Eq. (20) because the numerical FFT destroys the positive definiteness of the metric. We tested the use of the FFT integrals in the other two equations as follows: (1) Using FFT reciprocal space quantities in the second term of Eq. (22), denoted MDF-FFT(1) in Figures 1a and 1b; (2) Using FFT reciprocal space quantities in both Eqs. (22) and (23), denoted MDF-FFT(2). To illustrate the density sampling error when using the FFT, we also computed the PW related integrals using AFT, and the pure AFT results are also presented in Figures 1a and 1b. MDF-FFT(1) gives a similar error to pure PW density fitting (using FFT for the PW related integrals) because the errors from the FFT density sampling is larger than the corrections introduced by the Gaussian fitting functions in MDF. The error in MDF-FFT(2) is more severe, as the numerical errors introduced by the FFT are compounded in Eqs. (22) and (23). In either case, the use of the FFT to approximate the quantities involved in MDF clearly leads to unacceptable errors.

Figure 2 shows the convergence of Γ -point all-electron Hartree-Fock energies for the

silicon crystal (Fd $\bar{3}$ m symmetry, lattice parameter $a = 5.431$ Å, cc-pVDZ basis). We used a large ETB fitting basis *20s16p13d7f2g* (see Table 1). The exponents of the compensating Gaussians were set to 0.2, and the real space lattice sums were truncated at 12 Å. We use this system to test the effect of the linear dependency threshold, and linear thresholds of 10^{-9} , 10^{-8} and 10^{-7} were used, keeping all other settings the same.

Because of the large Gaussian fitting basis, the GDF method achieves good accuracy for the total energy. This is close to the accuracy of the MDF method with 125 PWs (corresponding to a PW energy cutoff of 20 eV). In this system, the presence of core functions means that PWs alone are insufficient to expand the densities; however, when used in conjunction with Gaussians, MDF systematically improves beyond the GDF result. However, we observe that the linear dependency threshold in MDF can strongly affect the accuracy of the HF energy. With exact arithmetic, a tighter linear dependence threshold, which retains more fitting functions, should produce more accurate results. However, for a small number of PWs, the thresholds 10^{-9} and 10^{-8} in fact introduce large errors, due to the numerical instability associated with the linear dependence between diffuse Gaussians and PWs. Thus although more diffuse fitting functions are removed by the looser threshold, the numerical problems are less severe and better accuracy is achieved. Taking the MDF basis with 729 PWs (energy cutoff 80 eV) as an example, a threshold of 10^{-9} retains 1471 fitting functions out of the original 1600 auxiliary Gaussian functions and gives an error of 10 mE_h , while a threshold of 10^{-7} retains 1312 linearly independent fitting functions and gives an error of only 0.01 mE_h . However, when higher energy PWs are included in the MDF expansion, more diffuse Gaussians are removed by the threshold, and the PW functions increasingly take over the role of expanding the diffuse density. In this case, the numerical issues become relatively less serious and the different thresholds produce similar convergence, since the linear dependence between the steep Gaussian functions and the PWs is weak. For example, with 24389 PWs (energy cutoff 1000 eV) in MDF, a threshold of 10^{-9} leads to 944 linearly independent auxiliary Gaussian functions, and a threshold of 10^{-7} leads to 888 functions.

As discussed in the introduction, an important motivation for all-electron calculations enabled by MDF is that they allow us to assess pseudo-potential error. We now briefly examine the pseudo-potential error in the band structure of the silicon crystal. Figure 3 presents the LDA bands computed within a pseudopotential (PP) and an all-electron calculation using a $6 \times 6 \times 6$ k -point mesh with two atoms per (primitive) unit cell. In the PP calculation, we used the GTH pseudopotentials^{33,34} that were optimized for the LDA functional and the GTH DZVP basis, obtained from the CP2K^{26,35} software package. The PP Coulomb integrals were computed with 3375 PWs (energy cutoff 750 eV) using FFT. In the all-electron calculation, we used the cc-pVDZ AO basis and a fitting basis consisting of the ETB basis *20s16p13d7f2g* and 1331 PWs (energy cutoff 380 eV). The valence bands and conduction bands agree very well between the two types of calculations near the Fermi level, although quantitative discrepancies appear further from the Fermi level. The band gap of the PP calculation is 0.72 eV while the all electron calculation predicts a band gap of 0.69 eV.

Last, we briefly compare the computational cost of the MDF method in all-electron and pseudo-potential calculations to our earlier Gaussian orbital FFT-based pseudo-potential algorithm.^{31,32} In the FFT-based DFT calculation, evaluating the Gaussian AO values on the real-space mesh grid is the expensive operation with a formal scaling of $O(nN_GN_c)$. As shown in Section 2.1, the scaling of the AFT in the MDF integrals is n times higher than the scaling of AO evaluation. In addition to the analytical Fourier transforms, the MDF method also requires the three-index Gaussian integrals, and these are computationally demanding as well. In the applications to the silicon crystal test system above using pseudopotentials, we found that the cost of the pseudo-potential MDF calculation was about an order of magnitude higher than the pseudo-potential FFT-based calculation. This reflects the fact that the Gaussian fitting basis is not really required to represent purely smooth densities. However, the strength of the MDF procedure is to enable all-electron calculations, and the all-electron calculations using the pure FFT algorithm would be prohibitively (orders of

magnitude more) expensive than with the MDF implementation.

4 Conclusions

In this work, we presented a Gaussian and plane-wave mixed density fitting (MDF) to compute electron repulsion integrals and associated quantities such as the Coulomb and exchange energies in periodic systems. Our algorithm possesses several new features, including the use of analytical Fourier transforms instead of the standard Fast Fourier Transform to achieve high accuracy, and an efficient transformation to remove linear dependencies between Gaussians and PWs.

MDF allows for periodic calculations both with pseudo-potentials and with all electrons. Compared to conventional GDF, the main advantage of MDF is the ability to systematically converge to high accuracy through the PW part of the expansion with a relatively weak dependence on the quality of the Gaussian fitting basis, and without the need for diffuse Gaussian fitting functions. The main disadvantage of the technique is the overhead incurred from handling the (relatively) large PW fitting basis. This means that the MDF approach is unlikely to be the method of choice for low-accuracy, or pseudo-potential calculations. However, for high accuracy all-electron calculations in large systems, MDF provides an efficient computational choice. Further, it is possible to accelerate MDF calculations by exploiting the dual sparsity of the densities in real and reciprocal space. These optimizations will be considered in our future work.

Appendix A Analytical integrals for periodic Gaussian functions

The integrals we presented in Section 2.1 can be evaluated analytically with real space lattice sums. For a crystal-momentum-conserving AO basis ($\mathbf{k}_\mu = \mathbf{k}_\nu$), the AO overlap integrals

(per unit cell) can be computed as

$$\begin{aligned}
S_{\mu\nu} &= \frac{1}{N} \langle \phi_\mu | \phi_\nu \rangle = \frac{1}{N} \int \sum_{\mathbf{T}_\mu} e^{-i\mathbf{k}_\mu \cdot \mathbf{T}_\mu} \mu^*(\mathbf{r} - \mathbf{T}_\mu) \sum_{\mathbf{T}_\nu} e^{i\mathbf{k}_\nu \cdot \mathbf{T}_\nu} \nu(\mathbf{r} - \mathbf{T}_\nu) d\mathbf{r} \\
&= \frac{1}{N} \int \sum_{\mathbf{T}_\mu} e^{-i\mathbf{k}_\mu \cdot \mathbf{T}_\mu} \mu^*(\mathbf{r} - \mathbf{T}_\mu) \sum_{\mathbf{T}_\nu} e^{i\mathbf{k}_\nu \cdot (\mathbf{T}_\nu + \mathbf{T}_\mu)} \nu(\mathbf{r} - \mathbf{T}_\mu - \mathbf{T}_\nu) d\mathbf{r} \\
&= \frac{1}{N} \sum_{\mathbf{T}_\mu} e^{i(\mathbf{k}_\nu - \mathbf{k}_\mu) \cdot \mathbf{T}_\mu} \int \sum_{\mathbf{T}_\nu} \mu^*(\mathbf{r}) e^{i\mathbf{k}_\nu \cdot \mathbf{T}_\nu} \nu(\mathbf{r} - \mathbf{T}_\nu) d\mathbf{r} \\
&= \int \sum_{\mathbf{T}_\nu} \mu^*(\mathbf{r}) e^{i\mathbf{k}_\nu \cdot \mathbf{T}_\nu} \nu(\mathbf{r} - \mathbf{T}_\nu) d\mathbf{r}
\end{aligned}$$

A similar treatment can be used for the other Gaussian integrals and Fourier transforms

$$\begin{aligned}
(\phi_P^{-\mathbf{k}} | \phi_Q^{\mathbf{k}}) &= \int \phi_P^{-\mathbf{k}}(\mathbf{r}_1) \frac{1}{r_{12}} \phi_Q^{\mathbf{k}}(\mathbf{r}_2) d\mathbf{r}_1 d\mathbf{r}_2 \\
&= \sum_{\mathbf{T}} e^{i\mathbf{k} \cdot \mathbf{T}} \int [\chi_P(\mathbf{r}_1) - \xi_P(\mathbf{r}_1)] \frac{1}{r_{12}} [\chi_Q(\mathbf{r}_2 - \mathbf{T}) - \xi_Q(\mathbf{r}_2 - \mathbf{T})] d\mathbf{r}_1 d\mathbf{r}_2
\end{aligned}$$

$$\begin{aligned}
(\phi_P^{-\mathbf{k}_{\kappa\lambda}} | \phi_\mu \phi_\nu) &= \frac{1}{\sqrt{N}} \int \phi_P^{-\mathbf{k}_{\kappa\lambda}}(\mathbf{r}_1) \frac{1}{r_{12}} \phi_\mu^*(\mathbf{r}_2) \phi_\nu(\mathbf{r}_2) d\mathbf{r}_1 d\mathbf{r}_2 \\
&= \sum_{\mathbf{T}_\mu \mathbf{T}_\nu} e^{i\mathbf{k}_\nu \cdot \mathbf{T}_\nu - i\mathbf{k}_\mu \cdot \mathbf{T}_\mu} \int [\chi_P(\mathbf{r}_1) - \xi_P(\mathbf{r}_1)] \frac{1}{r_{12}} \mu^*(\mathbf{r}_2 - \mathbf{T}_\mu) \nu(\mathbf{r}_2 - \mathbf{T}_\nu) d\mathbf{r}_1 d\mathbf{r}_2
\end{aligned}$$

$$\begin{aligned}
\rho_P(\mathbf{G} + \mathbf{k}) &= \frac{1}{\sqrt{N}} \int e^{-i(\mathbf{G} + \mathbf{k}) \cdot \mathbf{r}} \phi_P^{\mathbf{k}}(\mathbf{r}) d\mathbf{r} \\
&= \frac{1}{N} \int e^{-i(\mathbf{G} + \mathbf{k}) \cdot \mathbf{r}} \sum_{\mathbf{T}} e^{i\mathbf{k} \cdot \mathbf{T}} [\chi_P(\mathbf{r} - \mathbf{T}) - \xi_P(\mathbf{r} - \mathbf{T})] d\mathbf{r} \\
&= \frac{1}{N} \int \sum_{\mathbf{T}} e^{-i(\mathbf{G} + \mathbf{k}) \cdot (\mathbf{r} + \mathbf{T})} e^{i\mathbf{k} \cdot \mathbf{T}} [\chi_P(\mathbf{r}) - \xi_P(\mathbf{r})] d\mathbf{r} \\
&= \int e^{-i(\mathbf{G} + \mathbf{k}) \cdot \mathbf{r}} [\chi_P(\mathbf{r}) - \xi_P(\mathbf{r})] d\mathbf{r}
\end{aligned}$$

$$\rho_{\mu\nu}(\mathbf{G} + \mathbf{k}_{\mu\nu}) = \int e^{-i(\mathbf{G} + \mathbf{k}_{\mu\nu}) \cdot \mathbf{r}} \phi_\mu^*(\mathbf{r}) \phi_\nu(\mathbf{r}) d\mathbf{r}$$

$$\begin{aligned}
&= \frac{1}{N} \int e^{-i(\mathbf{G}+\mathbf{k}_{\mu\nu})\cdot\mathbf{r}} \sum_{\mathbf{T}_\mu} e^{-i\mathbf{k}_\mu\cdot\mathbf{T}_\mu} \mu^*(\mathbf{r}-\mathbf{T}_\mu) \sum_{\mathbf{T}_\nu} e^{i\mathbf{k}_\nu\cdot\mathbf{T}_\nu} \nu(\mathbf{r}-\mathbf{T}_\nu) d\mathbf{r} \\
&= \frac{1}{N} \int \sum_{\mathbf{T}_\mu} e^{-i(\mathbf{G}+\mathbf{k}_{\mu\nu})\cdot(\mathbf{r}+\mathbf{T}_\mu)} e^{-i\mathbf{k}_\mu\cdot\mathbf{T}_\mu} \mu^*(\mathbf{r}) \sum_{\mathbf{T}_\nu} e^{i\mathbf{k}_\nu\cdot(\mathbf{T}_\mu+\mathbf{T}_\nu)} \nu(\mathbf{r}-\mathbf{T}_\nu) d\mathbf{r} \\
&= \sum_{\mathbf{T}_\nu} e^{i\mathbf{k}_\nu\cdot\mathbf{T}_\nu} \int e^{-i(\mathbf{G}+\mathbf{k}_{\mu\nu})\cdot\mathbf{r}} \mu^*(\mathbf{r}) \nu(\mathbf{r}-\mathbf{T}_\nu) d\mathbf{r}
\end{aligned}$$

Integral (14) is computed as

$$\begin{aligned}
\bar{V}_P^{\mathbf{k}} &= \lim_{N \rightarrow \infty} \frac{1}{\sqrt{N}} \int \frac{\phi_Q^{\mathbf{k}}(\mathbf{r}_2)}{r_{12}} d\mathbf{r}_1 d\mathbf{r}_2 \\
&= \lim_{N \rightarrow \infty} \frac{1}{N} \sum_{\mathbf{T}} e^{i\mathbf{k}\cdot\mathbf{T}} \int \frac{\chi_P(\mathbf{r}_2) - \xi_P(\mathbf{r}_2)}{r_{12}} d\mathbf{r}_1 d\mathbf{r}_2
\end{aligned}$$

The limits of this integral are non-vanishing only if $\mathbf{k} = 0$ and the integrands χ_P and ξ_P are of s -type spherical symmetry

$$\begin{aligned}
\bar{V}_P^{\mathbf{k}} &= \int \frac{1}{r_{12}} \left[\left(\frac{\alpha_{P_\chi}}{\pi} \right)^{3/2} e^{-\alpha_{P_\chi} |\mathbf{r}_2 - \mathbf{R}|^2} - \left(\frac{\alpha_{P_\xi}}{\pi} \right)^{3/2} e^{-\alpha_{P_\xi} |\mathbf{r}_2 - \mathbf{R}|^2} \right] d\mathbf{r}_1 d\mathbf{r}_2 \\
&= \frac{1}{(2\pi)^3} \int \int e^{i\mathbf{G}\cdot\mathbf{r}_1} d\mathbf{r}_1 \frac{4\pi}{G^2} \left(e^{-\frac{G^2}{4\alpha_{P_\chi}}} e^{-i\mathbf{G}\cdot\mathbf{R}} - e^{-\frac{G^2}{4\alpha_{P_\xi}}} e^{-i\mathbf{G}\cdot\mathbf{R}} \right) d\mathbf{G} \\
&= \int \delta(\mathbf{G}) \frac{4\pi}{G^2} \left(e^{-\frac{G^2}{4\alpha_{P_\chi}}} - e^{-\frac{G^2}{4\alpha_{P_\xi}}} \right) e^{-i\mathbf{G}\cdot\mathbf{R}} d\mathbf{G} \\
&= \lim_{G \rightarrow 0} \frac{4\pi}{G^2} \frac{e^{-\frac{G^2}{4\alpha_{P_\chi}}} - e^{-\frac{G^2}{4\alpha_{P_\xi}}}}{e^{i\mathbf{G}\cdot\mathbf{R}}} \\
&= \frac{\pi}{\alpha_{P_\xi}} - \frac{\pi}{\alpha_{P_\chi}}
\end{aligned}$$

Appendix B Analytical Fourier transformation

We applied analytical Fourier transformations in this work to guarantee the accuracy of the two-electron integrals. Given Gaussian functions

$$\mu(\mathbf{r}) = C_\mu (x - R_{x\mu})^{m_x} (y - R_{y\mu})^{m_y} (z - R_{z\mu})^{m_z} e^{-\alpha_\mu |\mathbf{r} - \mathbf{R}_\mu|^2},$$

$$\nu(\mathbf{r}) = C_\nu (x - R_{x\nu})^{n_x} (y - R_{y\nu})^{n_y} (z - R_{z\nu})^{n_z} e^{-\alpha_\nu |\mathbf{r} - \mathbf{R}_\nu|^2},$$

analytical Fourier transformations for the Gaussian function products can be computed as the products of three Cartesian components

$$\int e^{-i\mathbf{G}\cdot\mathbf{r}} \mu^*(\mathbf{r}) \nu(\mathbf{r}) d\mathbf{r} = C_\mu C_\nu I_{m_x, n_x}^x I_{m_y, n_y}^y I_{m_z, n_z}^z,$$

$$I_{m_x, n_x}^x = \int e^{-iG_x x} (x - R_{x\mu})^{m_x} e^{-\alpha_\mu (x - R_{x\mu})^2} (x - R_{x\nu})^{n_x} e^{-\alpha_\nu (x - R_{x\nu})^2} dx.$$

Each Cartesian component can be evaluated through the recursive relations

$$I_{0,0}^x = \sqrt{\frac{\pi}{\alpha_\mu + \alpha_\nu}} e^{-\frac{\alpha_\mu \alpha_\nu}{\alpha_\mu + \alpha_\nu} (R_{x\mu} - R_{x\nu})^2} e^{-\frac{G_x^2}{4(\alpha_\mu + \alpha_\nu)}} e^{-iG_x X_{\mu\nu}}$$

$$I_{1,0}^x = - \left(R_{x\mu} - X_{\mu\nu} + \frac{iG_x}{2(\alpha_\mu + \alpha_\nu)} \right) I_{0,0}^x$$

$$I_{m_x,0}^x = \frac{m_x - 1}{2(\alpha_\mu + \alpha_\nu)} I_{m_x-2,0}^x - \left(R_{x\mu} - X_{\mu\nu} + \frac{iG_x}{2(\alpha_\mu + \alpha_\nu)} \right) I_{m_x-1,0}^x$$

$$I_{m_x, n_x}^x = I_{m_x+1, n_x-1}^x + (R_{x\mu} - R_{x\nu}) I_{m_x, n_x-1}^x$$

where

$$X_{\mu\nu} = \frac{\alpha_\mu R_{x\mu} + \alpha_\nu R_{x\nu}}{\alpha_\mu + \alpha_\nu}.$$

References

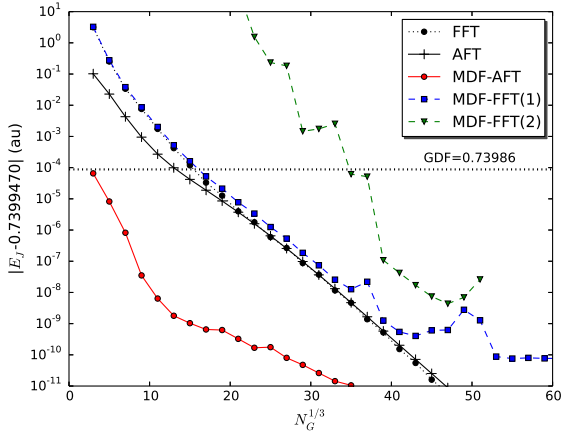
- (1) Whitten, J. L. J. Chem. Phys. **1973**, 58, 4496–4501.
- (2) Dunlap, B. I.; Connolly, J. W. D.; Sabin, J. R. J. Chem. Phys. **1979**, 71, 3396–3402.
- (3) Vahtras, O.; Almlöf, J.; Feyereisen, M. Chem. Phys. Lett. **1993**, 213, 514 – 518.
- (4) Eichkorn, K.; Treutler, O.; Öhm, H.; Häser, M.; Ahlrichs, R. Chem. Phys. Lett. **1995**, 240, 283 – 290.
- (5) Dunlap, B. I. Phys. Chem. Chem. Phys. **2000**, 2, 2113–2116.
- (6) Beebe, N. H. F.; Linderberg, J. Int. J. Quantum Chem. **1977**, 12, 683–705.
- (7) Røeggen, I.; Wisløff-Nilssen, E. Chem. Phys. Lett. **1986**, 132, 154 – 160.
- (8) Aquilante, F.; Gagliardi, L.; Pedersen, T. B.; Lindh, R. J. Chem. Phys. **2009**, 130, 154107.
- (9) Füsti-Molnar, L.; Pulay, P. J. Chem. Phys. **2002**, 116, 7795–7805.
- (10) Füsti-Molnar, L. J. Chem. Phys. **2003**, 119, 11080–11087.
- (11) Lippert, G.; Hutter, J.; Parrinello, M. Mol. Phys. **1997**, 92, 477–488.
- (12) Lippert, G.; Hutter, J.; Parrinello, M. Theor. Chem. Acc. **1999**, 103, 124–140.
- (13) Füsti-Molnar, L.; Kong, J. J. Chem. Phys. **2005**, 122, 074108.
- (14) Murphy, R. B.; Cao, Y.; Beachy, M. D.; Ringnalda, M. N.; Friesner, R. A. J. Chem. Phys. **2000**, 112, 10131–10141.
- (15) Neese, F.; Wennmohs, F.; Hansen, A.; Becker, U. Chem. Phys. **2009**, 356, 98 – 109.
- (16) Feyereisen, M.; Fitzgerald, G.; Komornicki, A. Chem. Phys. Lett. **1993**, 208, 359 – 363.

- (17) Komornicki, A.; Fitzgerald, G. J. Chem. Phys. **1993**, 98, 1398–1421.
- (18) Weigend, F.; Hser, M.; Patzelt, H.; Ahlrichs, R. Chem. Phys. Lett. **1998**, 294, 143 – 152.
- (19) Sierka, M.; Hogeekamp, A.; Ahlrichs, R. J. Chem. Phys. **2003**, 118, 9136–9148.
- (20) Manby, F. R.; Knowles, P. J.; Lloyd, A. W. J. Chem. Phys. **2001**, 115, 9144–9148.
- (21) Werner, H.-J.; Manby, F. R.; Knowles, P. J. J. Chem. Phys. **2003**, 118, 8149–8160.
- (22) Sodt, A.; Subotnik, J. E.; Head-Gordon, M. J. Chem. Phys. **2006**, 125.
- (23) Werner, H.-J.; Manby, F. R. J. Chem. Phys. **2006**, 124, 054114.
- (24) Jung, Y.; Sodt, A.; Gill, P. M. W.; Head-Gordon, M. Proc. Natl. Acad. Sci. U. S. A. **2005**, 102, 6692–6697.
- (25) Krack, M.; Parrinello, M. Phys. Chem. Chem. Phys. **2000**, 2, 2105–2112.
- (26) VandeVondele, J.; Krack, M.; Mohamed, F.; Parrinello, M.; Chassaing, T.; Hutter, J. Comput. Phys. Comm. **2005**, 167, 103–128.
- (27) Füsti-Molnar, L.; Pulay, P. J. Chem. Phys. **2002**, 117, 7827–7835.
- (28) Dovesi, R.; Civalieri, B.; Roetti, C.; Saunders, V. R.; Orlando, R. Rev. in Comput. Chem.; John Wiley & Sons, Inc., 2005; pp 1–125.
- (29) Kolafa, J.; Perram, J. W. Mol. Simul. **1992**, 9, 351–368.
- (30) Gibbon, P.; Sutmann, G. Lecture Notes, J. Grotendorst, D. Marx, A. Muramatsu (Eds.), John von Neumann Institute for Computing, Jlich, NIC Series; 2002; pp 467–506.
- (31) McClain, J.; Sun, Q.; Chan, G. K.-L.; Berkelbach, T. C. J. Chem. Theory Comput. **2017**, 13, 1209–1218.

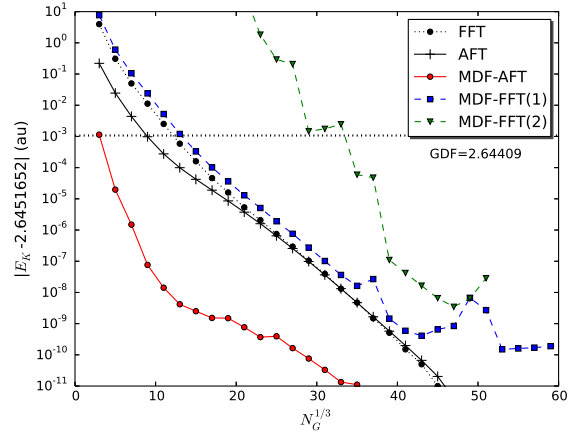
- (32) Sun, Q.; Berkelbach, T. C.; Blunt, N. S.; Booth, G. H.; Guo, S.; Li, Z.; Liu, J.; McClain, J.; Sayfutyarova, E. R.; Sharma, S.; Wouters, S.; Chan, G. K.-L. The Python-based Simulations of Chemistry Framework (PySCF). 2017.
- (33) Goedecker, S.; Teter, M.; Hutter, J. Phys. Rev. B **1996**, 54, 1703.
- (34) Hartwigsen, C.; Goedecker, S.; Hutter, J. Phys. Rev. B **1998**, 58, 3641.
- (35) Hutter, J.; Iannuzzi, M.; Schiffmann, F.; VandeVondele, J. WIREs: Comput. Mol. Sci. **2014**, 4, 15–25.

Table 1: Even-tempered basis, $\alpha\beta^i, i = 0, \dots, n - 1$

angular momentum	n	α	β
H atom $10s6p2d$			
s	10	0.244	1.6
p	6	0.596	1.6
d	2	1.454	1.6
Si atom $20s16p13d7f2g$			
s	20	0.333	1.8
p	16	0.324	1.8
d	13	0.316	1.8
f	7	0.310	1.8
g	2	0.550	1.8



(a) Coulomb energy for the H crystal



(b) Exchange energy for the H crystal

Figure 1: Coulomb and exchange interactions per unit cell for the H crystal (Γ point). In the H crystal, the reference energies are computed using a pure PW fitting basis and FFT computation of all terms with $N_G^{1/3} = 101$ grid points. The ETB basis $10s6p2d$ is employed for MDF and GDF.

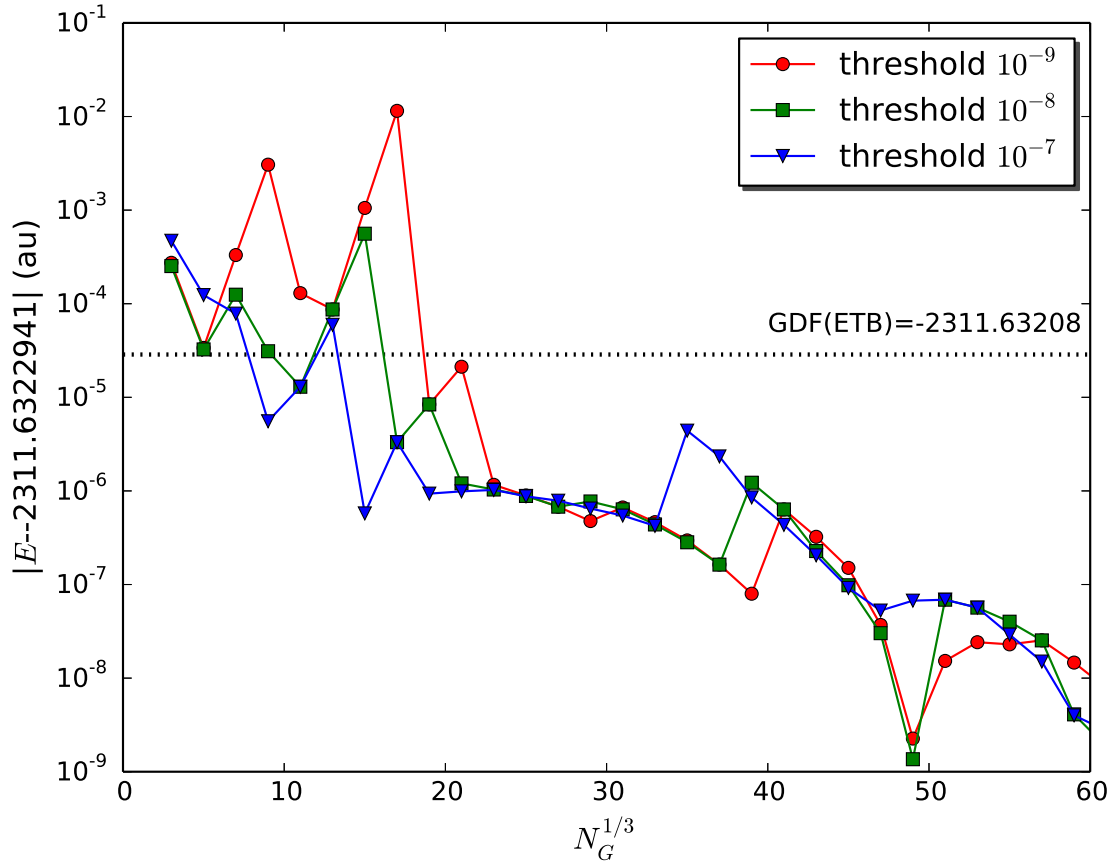


Figure 2: Hartree-Fock energy per unit cell for the Si crystal. The reference energies are computed using MDF with $N_G^{1/3} = 81$ grid points. The ETB basis is $20s16p13d7f2g$.

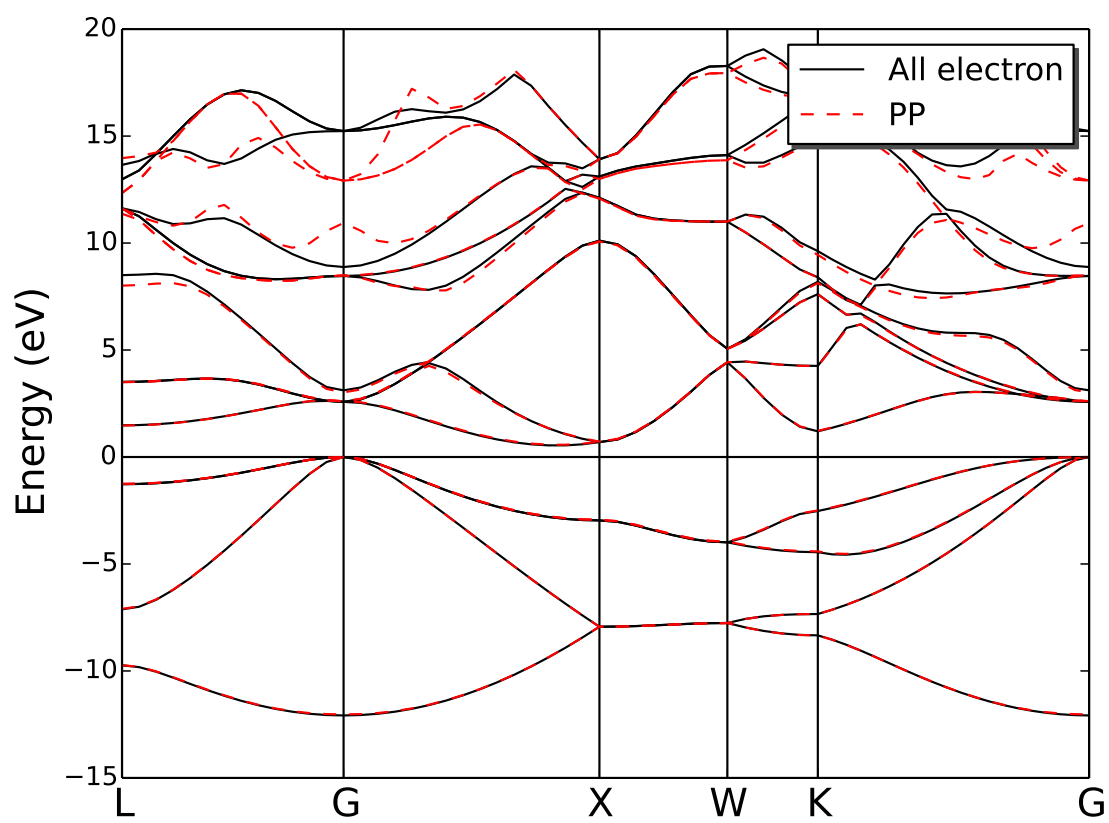


Figure 3: All-electron and pseudopotential LDA band structure of the Si crystal.